LETTER

doi:10.1038/nature24647

Discovery of a big void in Khufu's Pyramid by observation of cosmic-ray muons

Kunihiro Morishima[1], Mitsuaki Kuno[1], Akira Nishio[1], Nobuko Kitagawa[1], Yuta Manabe[1], Masaki Moto[1], Fumihiko Takasaki[2], Hirofumi Fujii[2], Kotaro Satoh[2], Hideyo Kodama[2], Kohei Hayashi[2], Shigeru Odaka[2], Sébastien Procureur[3], David Attié[3], Simon Bouteille[3], Denis Calvet[3], Christopher Filosa[3], Patrick Magnier[3], Irakli Mandjavidze[3], Marc Riallot[3], Benoit Marini[4], Pierre Gable[5], Yoshikatsu Date[6], Makiko Sugiura[7], Yasser Elshayeb[8], Tamer Elnady[9], Mustapha Ezzy[8], Emmanuel Guerriero[5], Vincent Steiger[4], Nicolas Serikoff[4], Jean-Baptiste Mouret[10,11,12], Bernard Charlès[13], Hany Helal[4,8] & Mehdi Tayoubi[4,13]

The Great Pyramid, or Khufu's Pyramid, was built on the Giza plateau in Egypt during the fourth dynasty by the pharaoh Khufu (Cheops)[1], who reigned from 2509 BC to 2483 BC. Despite being one of the oldest and largest monuments on Earth, there is no consensus about how it was built[2,3]. To understand its internal structure better, we imaged the pyramid using muons, which are by-products of cosmic rays that are only partially absorbed by stone[4–6]. The resulting cosmic-ray muon radiography allows us to visualize the known and any unknown voids in the pyramid in a non-invasive way. Here we report the discovery of a large void (with a cross-section similar to that of the Grand Gallery and a minimum length of 30 metres) situated above the Grand Gallery. This constitutes the first major inner structure found in the Great Pyramid since the nineteenth century[1]. The void, named ScanPyramids' Big Void, was first observed with nuclear emulsion films[7–9] installed in the Queen's chamber, then confirmed with scintillator hodoscopes[10,11] set up in the same chamber and finally re-confirmed with gas detectors[12] outside the pyramid. This large void has therefore been detected with high confidence by three different muon detection technologies and three independent analyses. These results constitute a breakthrough for the understanding of the internal structure of Khufu's Pyramid. Although there is currently no information about the intended purpose of this void, these findings show how modern particle physics can shed new light on the world's archaeological heritage.

The pyramid of Khufu is 139 m high and 230 m wide[1,13]. There are three known chambers (Fig. 1), at different heights of the pyramid, which all lie in the north–south vertical plane[1]: the subterranean chamber, the Queen's chamber, and the King's chamber. These chambers are connected by several corridors, the most notable one being the Grand Gallery (8.6 m high × 46.7 m long × 2.1–1.0 m wide). The Queen's

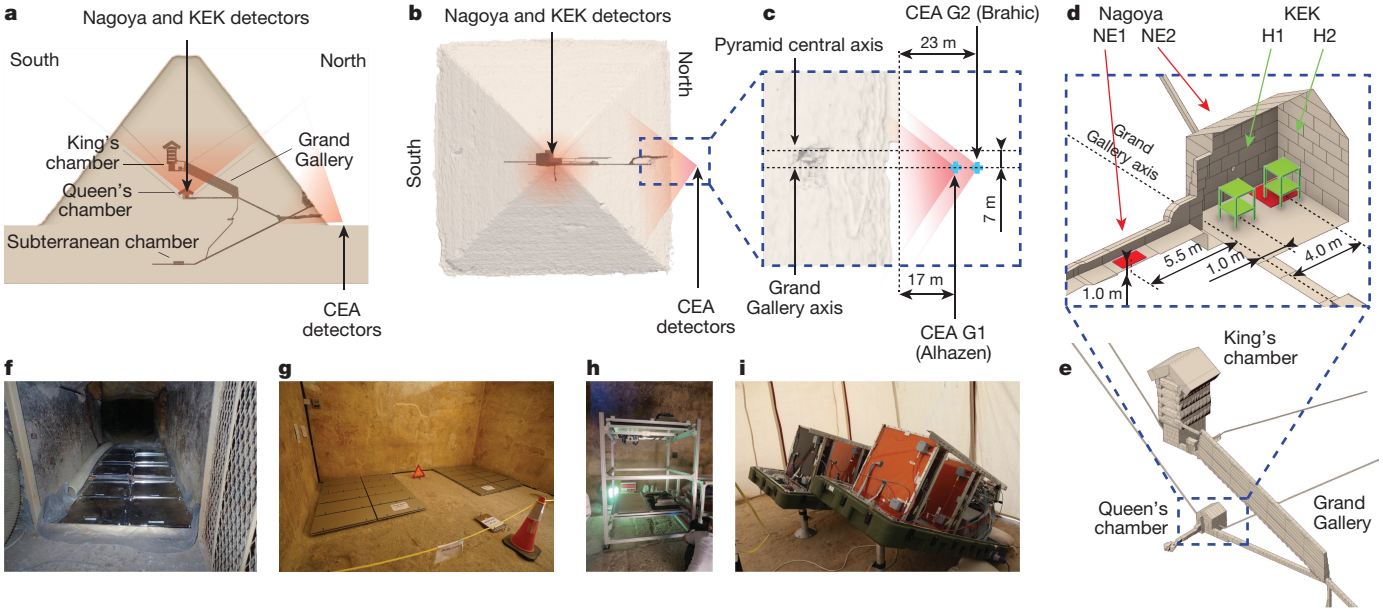

Figure 1 | Muon detectors installed for Khufu's Pyramid. a, Side view of the pyramid, with sensor positions and indicative field of view. **b**, Top view. **c**, Close view of the position of the gas detectors Brahic and Alhazen (CEA). **d**, Orthographic view of Queen's chamber with nuclear emulsion films (Nagoya University, red positions NE1 and NE2) and scintillator hodoscopes (KEK, green positions H1 and H2). **e**, Orthographic view of the main known internal structures. **f**, Nuclear emulsion plates in position NE1 (Nagoya University). **g**, Nuclear emulsion plates in position NE2 (Nagoya University). **h**, Scintillator hodoscope setup for position H1 (KEK). **i**, Gas detectors (muon telescopes, CEA).

[1]F-lab, Nagoya University, Furo-cho, Chikusa-ku, Nagoya, Aichi 464-8602, Japan. [2]High Energy Accelerator Research Organization (KEK), 1-1 oho, Tsukuba, Ibaraki 305-0801, Japan. [3]Institut de Recherche sur les lois Fondamentales de l'Univers (IRFU), Commissariat à l'Energie Atomique et aux Energies Alternatives (CEA), Université Paris Saclay, 91191 Gif-sur-Yvette, France. [4]HIP Institute, 50 rue de Rome, 75008 Paris, France. [5]Emissive, 71 rue de Provence, 75009 Paris, France. [6]NHK Enterprises, Inc. (NEP), 4-14 Kamiyama-cho, Shibuya-ku, Tokyo 150-0047, Japan. [7]Suave Images, N-2 Maison de Shino, 3-30-8 Kamineguro, Meguro-Ku, Tokyo 153-0051, Japan. [8]Cairo University, 9 Al Gameya, Oula, Giza Governorate, Egypt. [9]Ain Shams University, Kasr el-Zaafaran, Abbasiya, Cairo, Egypt. [10]Inria, Villers-lès-Nancy F-54600, France. [11]CNRS, Vandœuvre-lès-Nancy F-54500, France. [12]Université de Lorraine, Vandœuvre-lès-Nancy F-54500, France. [13]Dassault Systèmes, 10 Rue Marcel Dassault, 78140 Vélizy-Villacoublay, France.

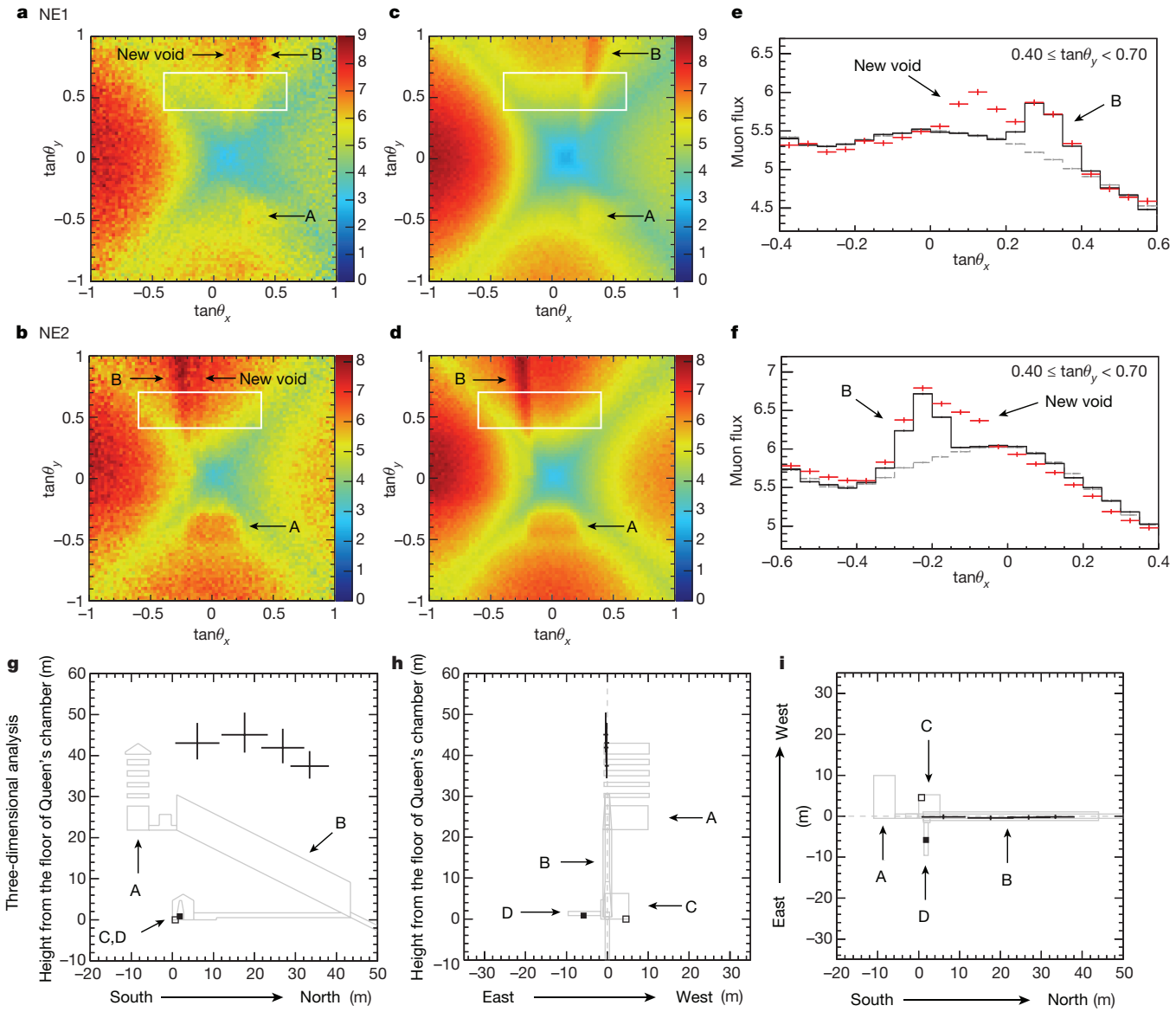

Figure 2 | Results of the analysis of the nuclear emulsion films. θ is the opening angle between the detected muon and the axis vertical to the detector. A indicates the King's chamber, B the Grand Gallery, C the Queen's chamber (position NE2), D the 'Niche' (position NE1) and 'New void' is the unexpected muon excess region. Right is west, top is north. **a**, **b**, Two-dimensional (2D) histograms of the detected muon flux (colour scale; muons per square centimetre per day per steradian) at positions NE1 and NE2. The resolution of this histogram is 0.025×0.025 (Methods). The four edges of the pyramid are clearly seen as a cross pattern. **c**, **d**, Results of Geant4 simulation[28] with the known inner structures from positions NE1 and NE2. **e**, **f**, Histograms of typical angular regions as shown by the white squares in **a**–**d** ($0.4 \leq \tan\theta_y < 0.7$). Data are shown in red; the black solid line is the simulation including the inner structures; and the grey dashed line is the simulation without the inner structures. Error bars indicate statistical error of 1σ (standard deviation). More slices are shown in Extended Data Fig. 2. **g**–**i**, Results of the triangulation analysis (three sectional views). Each figure shows the inner structures (grey lines) and the results. For each position, we divided the region of interest ($0 \leq \tan\theta_y < 1$) into four slices and extracted the centre of the muon excess for each of them, resulting in four pairs of directions (Methods). Each of the four points represents the result of the triangulation for a pair of slices and the associated statistical error (Methods). The detector positions are shown as filled black squares for position NE1 and open black squares for position NE2. **g** shows a vertical section (right is north); **h** shows a vertical section (right is west); and **i** shows a horizontal section (up is west, right is north).

chamber and the King's chamber possess two 'air shafts' each, which were mapped by a series of robots[14,15] between 1990 and 2010. The original entrance is believed to be the 'descending corridor', which starts from the north face, but today tourists enter the pyramid via a tunnel attributed to Caliph al-Ma'mun (around AD 820)[1].

Most of the current understanding of Khufu's Pyramid comes from architectural surveys and comparative studies with other pyramids[1,2,13]. In *Histories*, Herodotus described the construction of Khufu's Pyramid, but this account was written about 2,000 years later (in 440 BC). The only known documents written during Khufu's reign were discovered[16] in 2013, but these papyri describe only the logistics of the construction, such as how the stones were transported, and not the construction itself. In 1986, a team surveyed the pyramid using microgravimetry[17], that is, the measurement of slight variations in gravity due to large variations in the amount of matter[18]. Using these data, the team drilled three holes in the corridor to the Queen's chamber in the hope of finding a 'hidden chamber', but found only sand[17]. A more recent analysis of the same data dismissed the theory of a 'hidden chamber' where the holes had been drilled[17]. In 1988, a ground-penetrating radar survey[19] suggested that an unknown corridor could be parallel to the Queen's chamber corridor. To our knowledge, this theory has been neither confirmed nor refuted.

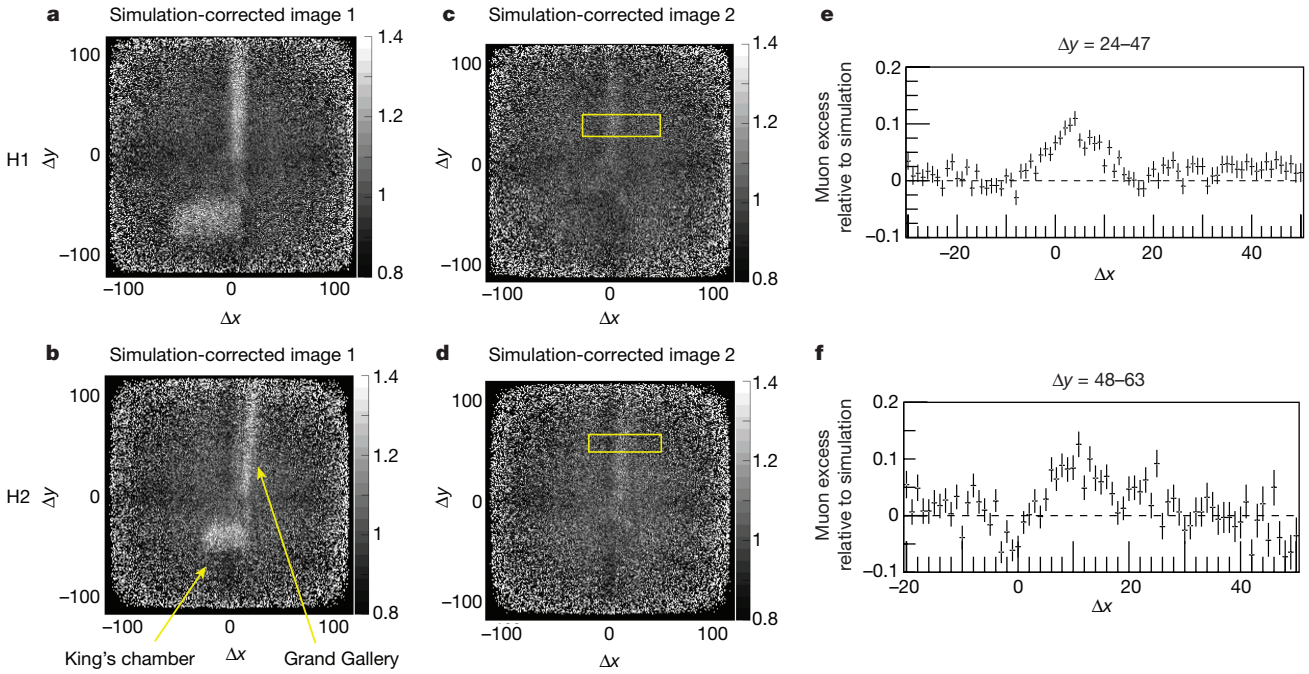

Figure 3 | Results of the analysis of the scintillation hodoscopes. **a**, **b**, 2D plots of the detected angle of muons after normalization by the simulation without inner structures at positions H1 and H2 (Methods). The images present a top view and north is up. Δx and Δy correspond to the channel number difference between the upper and lower layers along the x and y axes (Methods). The bin number hence ranges from −120 to 120 and provides the tangent of the incident angle when divided by 150 for position H1 and by 100 for position H2. The detector introduces a dark cross-shaped artefact visible on the 2D histograms, which adds a small systematic error of 3% to the analysis (Methods). **c**, **d**, 2D plots of the detected angle of muons after a normalization by the simulation with inner structures (which are hence removed). The images present a top view and north is up. The unexpected structure is visible. **e**, **f**, Histograms of the typical angular region ($-30 < \Delta x < 50$, $24 < \Delta y < 47$ for **e** and $-20 < \Delta x < 50$, $48 < \Delta y < 63$ for **f**) corresponding to a slice of **c** and **d** (yellow rectangles). More slices are shown in Extended Data Fig. 4. Black points with error bars show the relative excess after dividing the data by the model with the known structures (the King's chamber and the Grand Gallery): a perfect agreement between the data and the model would correspond to a horizontal line; a peak corresponds to an unexpected excess (relative to the simulation) of muons in the data.

Here we follow in the footsteps of Alvarez *et al.*[5], who used spark chambers as muon detectors in Khafre's Pyramid (Pyramid of Kephren) and concluded that there is no unknown structure with a volume similar to the King's chamber above the Belzoni chamber[5]. Muon particles originate from the interactions of cosmic rays with the atoms of the upper atmosphere, and they continuously reach the Earth with a speed near to that of light and a flux of around 10,000 muons per square metre per minute[4]. Like X-rays, which can penetrate the body and allow bone imaging, these elementary particles can maintain a quasi-linear trajectory through hundreds of metres of stone before decaying or being absorbed. By recording the position and the direction of each muon that traverses its detection surface, a muon detector can distinguish cavities from stone: while muons cross cavities with almost no interactions, they can be absorbed or deflected by stone. Thus, muons traversing a region with lower-than-expected density will result in a higher-than-expected flux in the direction of the region. In recent years, muon detectors have been successfully deployed in particle accelerators, in volcanology[6], to visualize the inner structure of the Fukushima nuclear reactor[11,20], and for homeland security[21]. In heritage buildings, detectors have been recently set up in archaeological sites near Rome[22] and Naples[23] (Italy), where they were able to detect some known structures from underground, and in the Teotihuacan Pyramid of the Sun (Mexico)[24]. However, since the muons generated by cosmic rays come from the sky, the detectors can detect density variations only in some solid angle above them (the exact acceptance depends on the detection technology). In addition, the muon imaging technique measures the average density of the structure in a given direction, so although a void has much lower density, its impact on the flux of muons is determined by the ratio between the void and the length of material that is traversed. For this reason, small cavities like air shafts cannot be detected by this technique within a reasonable exposure time. Lastly, in large and dense buildings like Khufu's Pyramid where only about 1% of muons reach the detectors, the data need to be accumulated over several months.

We first used nuclear emulsion films (Fig. 1f and g), developed by Nagoya University, because they are compact and do not require electric power, which makes them well suited for installation in the pyramid (Extended Data Table 1). A nuclear emulsion film is a special photographic film that can detect muon trajectories in three-dimensional (3D) images with sub-micrometre accuracy[7–9]. In these experiments, we used unit films of 30 cm × 25 cm and covered a maximum of 8 m^2 at a time. Each film has a 70-μm-thick emulsion coating on both sides of a 175-μm-thick transparent plastic base (Methods). The muon measurement accuracy is around 1 μm in position and around 1.8 mrad (about 0.1°) for the vertical track when using the information obtained with one film (Extended Data Table 1).

The films were installed near the southwest corner of the Queen's chamber (nuclear emulsion film position NE2, Fig. 1d and g) and in the adjacent narrow hand-excavated corridor called 'Niche' (position NE1, Fig. 1d and f) on the east side of the Queen's chamber. The distance between the centres of these two detectors is about 10 m, which allows us to perform a stereo analysis of the detected structures. The exposure started in December 2015. During the exposure, we modified the film configuration several times when we changed the films (about every two months); only a subset of the full dataset was used for this analysis to mitigate the effect of the parallax on the resolution (Extended Data Table 1 and Methods). After each exposure, the nuclear emulsion films were processed by photographic development in the darkroom of the Grand Egyptian Museum Conservation Center. After development,

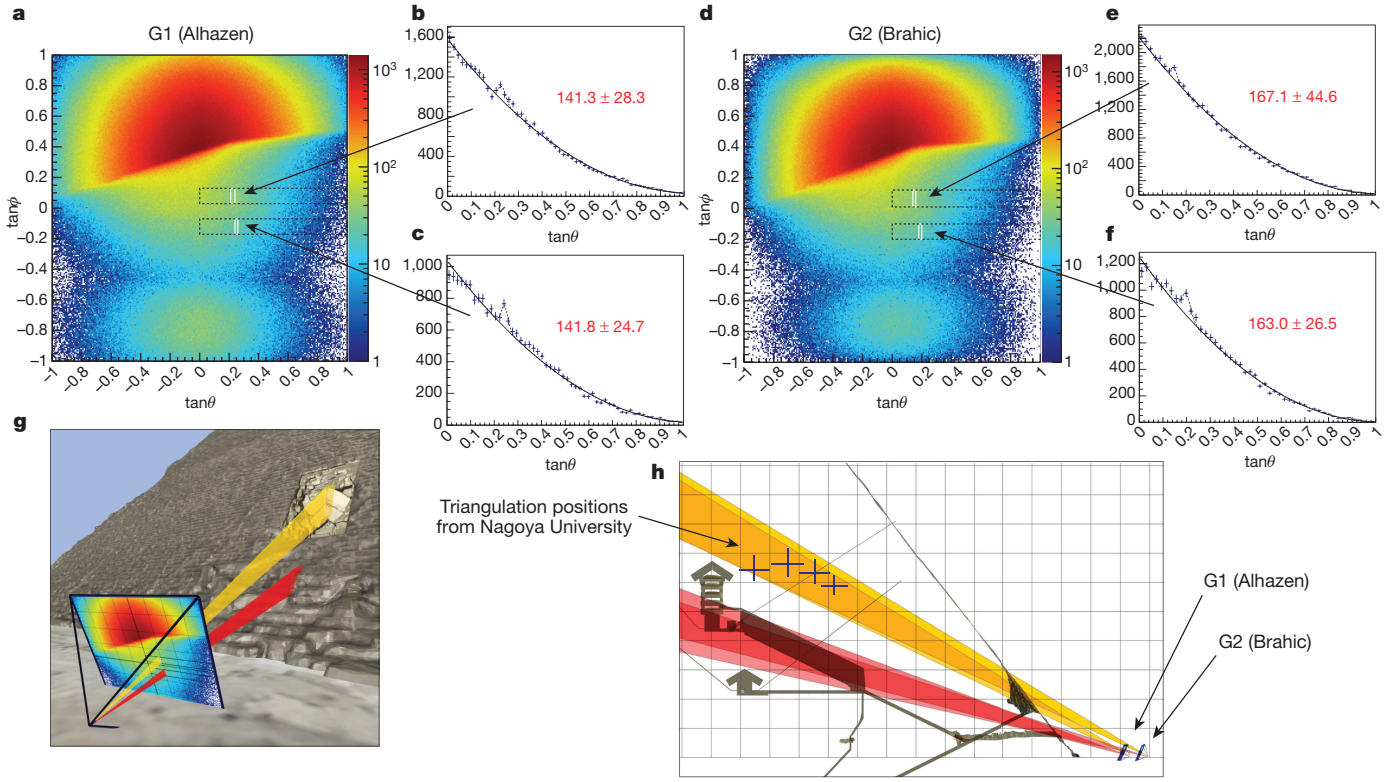

Figure 4 | Results of the analysis of the gas detectors. a, 2D image from position G1 (Alhazen telescope, Fig. 1a and b) in logarithmic scale, with white rectangles indicating the two muon flux excesses seen by the telescope. **b**, **c**, Horizontal slices showing the muon flux excess that corresponds to the upper (**b**) and lower (**c**) dotted black rectangles in **a**. The solid black lines are fits to the data (Methods). **d**, 2D image from position G2 (Brahic telescope, Fig. 1a and b) in logarithmic scale, with white rectangles indicating the two muon flux excesses seen by the telescope. Some noise is visible at the centre of the image, but it does not interfere with the scanned regions. **e**, **f**,Horizontal slices showing the muon flux excess that corresponds to the upper (**e**) and lower (**f**) black rectangles in **d**. **g**, Yellow cone and red cone, traced from position 1, indicating the angular area for the observed muon excesses (**a**–**c**). The two cones intersect the vertical plane of the Grand Gallery (Real-Time Muography Simulator, RTMS, software). **h**, Side view of the same cones as in **g**, for the two positions, confirming that the two muon flux excesses correspond to the Grand Gallery and the new void. The black crosses correspond to the position estimated with the nuclear emulsion plates (Fig. 2g–i): the two analyses are perfectly compatible. Grid size is 10 m (RTMS software). More slices are shown in Extended Data Fig. 6.

they were transported to Nagoya University and read out by an automated nuclear emulsion scanning system[25–27].

We compared the resulting muon radiographs (Fig. 2a and b) with the expected results computed using a Monte Carlo simulation that includes known structures inside the observation region (Fig. 2c and d). These comparisons clearly show that the large known structures (the Grand Gallery and the King's chamber) are observed by the measurements and the results match what is known (Fig. 2a–d). However, from the two positions, we also detected an unexpected and significant excess of muons in a region almost parallel to the image of the Grand Gallery. The statistical significance of the excess is higher than 10σ at the highest difference direction. The muon excess is similar to the one generated by the Grand Gallery, which means that the volume of the two voids is of the same order (Fig. 2e and f and Extended Data Fig. 2). We then performed triangulation using the data from the two positions and four points along the new void (Methods). The results show that the new void has an estimated length of more than 30 m and is located 40–50 m away from the detector positions, 21 m above the ground level (Fig. 2g–i).

The second detection technology, designed by the High Energy Accelerator Research Organization (KEK) is composed of four layers of scintillator hodoscopes arranged in two units of double orthogonal layers[10,11] (Fig. 1h). Each layer is composed of 120 plastic scintillator bars measuring 1 cm × 1 cm in cross-section to cover an area of 120 cm × 120 cm. Two units are vertically separated to allow the measurement of the 2D incoming direction of the muons. We placed the detectors near the southeast corner (position H1, Fig. 1d) of the Queen's chamber in August 2016. The separation between two units was set to 1.5 m. Unfortunately, the newly detected void was overlapping with the Grand Gallery, which made it difficult to identify. After stable operation for five months, we moved the detector to another position near the southwest corner of the chamber in January 2017 (position H2, 2.9 m from position H1, Fig. 1d) and reduced the unit separation to 1.0 m to enlarge the angular coverage of the measurement. The detector operation has been very stable for more than one year and is still continuing (Methods).

When we normalize the results by simulating the solid pyramid without the known structures, we can see the King's chamber and the Grand Gallery clearly (Fig. 3a and b). By normalizing with a simulation that includes the known structures, we observe a muon excess that is consistent with Nagoya University's result (Methods, Fig. 3c–f).

The third kind of instrument, designed by Commissariat à l'Energie Atomique et aux Energies Alternatives (CEA), is made of micropattern gaseous detectors (Micromegas) based on an argon mixture[12] (Methods). They are robust enough to be installed outside and can run for unlimited time, but they have a larger footprint than the emulsion plates (Fig. 1i, Extended Data Table 1). Each 'telescope' is built from four identical detectors with an active area of 50 cm × 50 cm, and a signal from at least three of them is required to trigger the acquisition. An online analysis is performed to extract the muon track parameters, which are then transferred to CEA, in France, with a 3G connection (Methods).

To confirm Nagoya University's discovery and to provide an additional point of view, we placed two such telescopes in front of the north

face of the pyramid (Fig. 1a–c), looking in the direction of the Grand Gallery (Methods), and close enough to each other that their data can be combined (Fig. 1c). A previous three-month measurement campaign with one telescope on the north side had already revealed an anomaly in this region, with statistical significance above 3σ, but the telescope was shifted from the main vertical axis, and so not optimally positioned. After two months of acquisition from the new position, the data analysis revealed two statistically significant excesses of muons in the core of the pyramid (Fig. 4): one corresponding to the Grand Gallery and one corresponding to the unexpected void (Methods). The 3D model confirms that the telescopes' observation converges to the same region as the region obtained from the emulsion plates in the Queen's chamber (Fig. 4h). The overall combined excesses yield 8.4σ for the Grand Gallery and 5.8σ for the new void (Methods). To our knowledge, this is the first time an instrument has detected a deep void from outside a pyramid.

Three techniques of cosmic-ray muon imaging were applied to investigate the inner structure of the pyramid. The known voids (the King's chamber and the Grand Gallery) were observed, as well as an unexpected big void, which demonstrates the ability of cosmic-ray muon radiography to image structures. There are still many architectural hypotheses to consider; in particular, the big void could consist of one or several adjacent voids, and it could be inclined or horizontal.

Online Content Methods, along with any additional Extended Data display items and Source Data, are available in the online version of the paper; references unique to these sections appear only in the online paper.

Received 12 October; accepted 24 October 2017.
Published online 2 November 2017.

1. Lehner, M. *The Complete Pyramids: Solving the Ancient Mysteries* (Thames and Hudson, 2008).
2. Hawass, Z. Pyramid construction: new evidence discovered in Giza. In *Stationen. Beiträge zur Kulturgeschichte Ägyptens Rainer Stadelmann gewidmet* (eds Guksch, H. & Polz, D.) 53–62 (Philipp von Zabern, 1998).
3. Smith, C. B., Hawass, Z. & Lehner, M. *How the Great Pyramid was Built* (Harper Collins, 2006).
4. Particle Data Group. Review of particle physics. *Chin. Phys.* **C40,** 100001 (2016).
5. Alvarez, L. W. *et al.* Search for hidden chambers in the pyramids. *Science* **167,** 832–839 (1970).
6. Tanaka, H. K. M., Nakano, T., Takahashi, S., Yoshida, J. & Niwa, K. Development of an emulsion imaging system for cosmic-ray muon radiography to explore the internal structure of a volcano, Mt. Asama. *Nucl. Instrum. Methods A* **575,** 489–497 (2007).
7. Morishima, K., Nishio, A., Moto, M., Nakano, T. & Nakamura, M., Development of nuclear emulsion for muography. *Ann. Geophys.* **60,** 0112 (2017).
8. Nakamura, T. A. *et al.* The OPERA film: new nuclear emulsion for large-scale, high-precision experiments. *Nucl. Instrum. Methods A* **556,** 80–86 (2006).
9. Nishio, A., Morishima, K., Kuwabara, K. & Nakamura, M. Development of nuclear emulsion detector for muon radiography. *Phys. Proc.* **80,** 74–77 (2015).
10. Fujii, H. *et al.* Detection of on-surface objects with an underground radiography detector system using cosmic-ray muons. *Progr. Theor. Exp. Phys.* **5,** 053C01 (2017).
11. Fujii, H. *et al.* Performance of a remotely located muon radiography system to identify the inner structure of a nuclear plant. *Progr. Theor. Exp. Phys.* **7,** 073C01 (2013).
12. Bouteille, S. *et al.* A Micromegas-based telescope for muon tomography: the WatTo experiment. *Nucl. Instrum. Methods A* **834,** 223–228 (2016).
13. Dash, G. The Great Pyramid's footprint: results from our 2015 survey. *Aeragram* **16,** 8–14 (2015).
14. Hawass, Z. *et al.* First report: video survey of the southern shaft of the Queen's chamber in the Great Pyramid. *Ann. Serv. Antiq. Egypte* **84,** 203–216 (2010).
15. Richardson, R. *et al.* The "Djedi" robot exploration of the southern shaft of the Queen's Chamber in the Great Pyramid of Giza, Egypt. *J. Field Robot.* **30,** 323–348 (2013).
16. Tallet, P. *Les Papyrus de la Mer Rouge 1 : Le "Journal de Merer"* http://www.ifao.egnet.net/publications/catalogue/9782724707069/ (Institut Français d'Archéologie Orientale, 2017).
17. Bui, H. D. *Imaging the Cheops Pyramid* (Springer Science & Business Media, 2011).
18. Butler, D. K. Microgravimetric and gravity gradient techniques for detection of subsurface cavities. *Geophysics* **49,** 1084–1096 (1984).
19. Yoshimura, S., Nakagawa, T., Tonouchi, S. & Seki, K. Non-destructive pyramid investigation. Parts 1 and 2. *Stud. Egypt. Cult.* **6 & 8,** http://www.egyptpro.sci.waseda.ac.jp/pdf%20files/SEC06%20Pyramid%20Investigation1.pdf and http://www.egyptpro.sci.waseda.ac.jp/pdf%20files/SEC08%20Pyramid%20Investigation2.pdf (1987).
20. Morishima, K. *et al.* First demonstration of cosmic ray muon radiography of reactor cores with nuclear emulsion based on an automated high-speed scanning technology. *Proc. 26th Worksh. on 'Radiation Detectors and Their Uses'* 27–36, https://lib-extopc.kek.jp/preprints/PDF/2012/1225/1225008.pdf (2012).
21. Borozdin, K. N. *et al.* Surveillance: radiographic imaging with cosmic-ray muons. *Nature* **422,** 277 (2003).
22. Menichelli, M. *et al.* A scintillating fibres tracker detector for archaeological applications. *Nucl. Instrum. Methods A* **572,** 262–265 (2007).
23. Saracino, G. *et al.* Imaging of underground cavities with cosmic-ray muons from observations at Mt. Echia (Naples). *Sci. Rep.* **7,** 1181 (2017).
24. Menchaca-Rocha, A. Searching for cavities in the Teotihuacan Pyramid of the Sun using cosmic muons experiments and instrumentation. *Int. Cosmic Ray Conf.* **4,** 325 (2011).
25. Yoshimoto, M., Nakano, T., Komatani, R. & Kawahara, H. Hyper-track selector nuclear emulsion readout system aimed at scanning an area of one thousand square meters. *Progr. Theor. Exp. Phys.* **10,** 103H01 (2017).
26. Morishima, K., Hamada, K., Komatani, R., Nakano, T. & Kodama, K. Development of an automated nuclear emulsion analyzing system. *Radiat. Meas.* **50,** 237–240 (2013).
27. Hamada, K. *et al.* Comprehensive track reconstruction tool "NETSCAN 2.0" for the analysis of the OPERA Emulsion Cloud Chamber. *J. Instrum.* **7,** P07001 (2012).
28. Agostinelli, S. *et al.* GEANT4—a simulation toolkit. *Nucl. Instrum. Methods A* **506,** 250–303 (2003).

Acknowledgements This experiment is part of the ScanPyramids project, which is supported by NHK, La Fondation Dassault Systèmes, Suez, IceWatch, le Groupe Dassault, Batscop, Itekube, Parrot, ILP, Kurtzdev, Gen-G and Schneider Electric. Measurement with nuclear emulsions was supported by the JST-SENTAN Program from the Japan Science and Technology Agency and JSPS KAKENHI (grant JP15H04241). The CEA telescopes were funded partly by the Région Ile-de-France and the P2IO LabEx (grant ANR-10-LABX-0038) in the framework 'Investissements d'Avenir' (grant ANR-11-IDEX-0003-01) managed by the Agence Nationale de la Recherche (France). The detectors were built by the ELVIA company and the CERN Micro-Pattern Gaseous Detector workshop. We thank the members and benefactors of the ScanPyramids project, and in particular: T. Hisaizumi, the members of Cairo University, the members of the F-laboratory in Nagoya University, Y. Doki, the Aïn El Shams University 3D scanning team, the members of the Egyptian Ministry of Antiquities, K. El Enany, M. El Damaty, T. Tawfik, S. Mourad, S. Tageldin, E. Badawy, M. Moussa, T. Yabuki, D. Takama, T. Shibasaki, K. Tsutsumida, K. Mikami, J. Nakao, H. Kurihara, S. Wada, H. Anwar, T. de Tersant, P. Forestier, L. Barthès, M.-P. Aulas, P. Daloz, S. Moignet, V. Raoult-Desprez, S. Sellam, P. Johnson, J.-M. Boursier, T. Alexandre, V. Ferret, T. Collet, H. Andorre, C. Oger-Chevalier, V. Picou, B. Duplat, K. Guilbert, J. Ulrich, D. Ulrich, C. Thouvenin, L. Jamet, A. Kiner, M.-H. Habert, B. Habert, L. Gaudé, F. Schuiten, F. Barati, P. Bourseiller, R. Theet, J.-P. Lutgen, R. Chok, N. Duteil, F. Tran, J.-P. Houdin, L. Kaltenbach, M. Léveillé-Nizerolle, R. Breitner, R. Fontaine, H. Pomeranc, F. Ruffier, G. Bourge, R. Pantanacce, M. Jany, L. Walker, L. Chapus, E. Galal, H. A. Mohalhal, S. M. Elhindawi, J. Lefaucheux, J.-M. Conan, E. M. Elwilly, A. Y. Saad, H. Barrada, E. Priou, S.Parrault, J.-C. Barré, X. Maldague, C. Ibarra Castenado, M. Klein, F. Khodayar, G. Amsellem, M. Sassen, C. Béhar, M. Ezzeldin, E. Van Laere, D. Leglu, B. Biard, N. Godin, P. der Manuelian, L. Gabriel, P. Attar, A. De Sousa, F. Morfoisse, R. Cotentin, C. Delache and G. Perrin.

Author Contributions K.M., M.K., A.N., N.K., Y.M. and M.M. performed the experiments and analysed the results for the nuclear emulsion films; F.T., H.F., K.S., H.K., K.H. and S.O. performed the experiments and analysed the results for the scintillator hodoscopes. S.P., D.A., S.B., D.C., C.F., P.M., I.M. and M.R. performed the experiment and analysed the results from the gas detector telescopes. B.M., P.G., E.G., N.S., Y.D. and M.S. created the 3D models used for the muography simulations and the RTMS. B.M. designed and implemented the RTMS and contributed to the analyses. Y.E., T.E., M.E. and V.S. coordinated the different experimental operations in the field (muography, 3D scans). The paper was mainly written by K.M., S.P., F.T., M.T., B.M. and J.-B.M., with contributions from all the other authors. H.H., M.T., B.C., B.M. and Y.E. designed and coordinated the project (ScanPyramids).

Author Information Reprints and permissions information is available at www.nature.com/reprints. The authors declare no competing financial interests. Readers are welcome to comment on the online version of the paper. Publisher's note: Springer Nature remains neutral with regard to jurisdictional claims in published maps and institutional affiliations. Correspondence and requests for materials should be addressed to K.M. (morishima@flab.phys.nagoya-u.ac.jp) and M.T. (tayoubi@hip.institute).

Reviewer Information *Nature* thanks G. Saracino, L. Thompson and the other anonymous reviewer(s) for their contribution to the peer review of this work.

METHODS

Nuclear emulsions from Nagoya University. *Detector design.* A nuclear emulsion is a special photographic film that is able to detect minimum ionizing particles such as cosmic-ray muons (Extended Data Fig. 1). The films used in this experiment were developed and produced at Nagoya University. In this design, silver bromide crystals with a diameter of 200 nm are dispersed in a 70-μm-thick sensitive emulsion layer, which is coated on both sides of a 175-μm-thick transparent polystyrene plastic base[7,29] (Extended Data Fig. 1a and b). When a charged particle passes through this emulsion layer, its 3D trajectory (track) is recorded and can be revealed through the chemical development process (Extended Data Fig. 1c and e). Thanks to the precise grain size and structure, tracks can be reconstructed with sub-micrometre accuracy in 4π steradians by using an optical microscope (Extended Data Fig. 1d). The track reconstruction quality depends on the grain density per length along the line of a track. In this experiment, films with a grain density of 37 grains per 100 μm and a noise level of about 1 grain per 1,000 μm^3 were used. These films can be used for long-term (2–3 months) measurement in an environment at 25 °C (temperature in the Queen's chamber) by tuning the volume occupancy of silver bromide crystals (35%)[30]. Each 30 cm × 25 cm film was vacuum-packed in an aluminium laminated package for light shielding and humidity control (30% relative humidity, RH) (Extended Data Fig. 1f). An acrylic plate with 2 mm thickness was also packed together for the control of noise increase[9]. The packed film was fixed onto an aluminium honeycomb plate (Extended Data Fig. 1g and h) at Nagoya University, and then transported to Cairo by aeroplane. To avoid the elevated cosmic-ray flux during the flight, we transported the two emulsion layers of each detector separately and assembled them in Egypt. Since we reject the trajectories that are not crossing the two layers, the muons accumulated during the flight are rejected in the analysis and are considered as background tracks.

Data acquisition. The observation with nuclear emulsion films was launched in the Queen's chamber in December 2015 and the films were periodically replaced. Each film was aligned with a reference line drawn with a laser marker and a spirit level, which led to an angular error of less than 10 mrad. After each exposure, we processed the films by photographic development in the dark room at the Grand Egyptian Museum Conservation Center. For the developing solution, we used the XAA developer (FUJI Film Co. Ltd) for 25 min at 20 °C. After development, we carried the films to Nagoya University, where they were read out by an automated nuclear emulsion scanning system developed since the early 1980s in Nagoya University[31,32]. In this experiment, tracks recorded in films were scanned by a Hyper Track Selector[25] which can read out tracks at a speed of 4,700 $cm^2\ h^{-1}$ with angular accuracy of 1.8 mrad for vertical tracks, and saved in a computer storage device as digital data (position, angle, pulse height). The angular acceptance is approximately $|\tan\theta| \leq 1.3$, where θ is the zenith angle relative to the perpendicular of the emulsion surface.

Data analysis and statistics. The muon tracks are reconstructed by the coincidence between the two stacked films within the criteria of signal selection and then counted as detected muons[26]. In this analysis, a subset of the full data set was used to avoid decreasing the resolution because of the imaging parallax: 4.4 million tracks were accumulated for 98 days at position NE1 and 6.2 million tracks for 140 days at position NE2, with an effective area of 0.45 m^2. Subsequently, detected muons were integrated into 2D angular space ($\tan\theta_x$–$\tan\theta_y$) with a bin size of a specified size (for example, 0.025 × 0.025) and angular acceptance of $|\tan\theta| \leq 1.0$, and converted to muon flux (muons per square centimetre per day per steradian) in each bin (Fig. 2a and b).

We used the Monte Carlo simulator Geant4 Version 10.2 (ref. 28) to compute the expected muon flux at the detector position. In these simulations, the physical processes of electromagnetic interactions and decays of muons were included, Miyake's formula[33] for the integrated intensity of cosmic-ray muons was used as a flux model, and only muons were generated as primary particles. To reduce the processing time, only muons were propagated and the range of incident muon energy was limited to 20–1,000 GeV in the zenith angular range 0°–70° ($-2.75 < \tan\theta < 2.75$). For the pyramid simulation, we modelled the shape and the location of the known structures (the Grand Gallery, the King's chamber, the corridor that connects them, and the Queen's chamber) using the survey of ref. 34. We defined that any void would be filled with air and that the stones are limestone (2.2 g cm^{-3}) except around the King's chamber, where they are granite (2.75 g cm^{-3}). The exposure period in the simulation is compatible with 1,000 days, which is approximately ten times longer than that of the analysed data. We estimated the 2D rock thickness distribution from the detector position: the minimum thickness is 65 m and the maximum thickness is 115 m. If we assume that the scale of the fluctuation of the surface structure is 1 m (stone size), the effect of the relative fluctuation is less than 2%.

Normalization was performed to compare real and simulated data in the region without the analysing target (the Grand Gallery, the King's chamber, and the anomaly region). The region of excess muon flux was clearly apparent in the images (Fig. 2a–d). Two histograms (Fig. 2e and f) show the muon flux extracted from the slice in $0.4 \leq \tan\theta_y < 0.7$. From the comparison between data and the simulation, the significances of each anomaly region were evaluated to be 13.7σ (statistical) for position NE1 and 12.7σ for position NE2.

To locate the anomalous structure, we performed triangulation from the two positions. The centre of the detector positioned at NE1 was located 5.8 m east of the axis of the Grand Gallery and 4.5 m west for position NE2. The distance between position NE1 and NE2 is 1.1 m north–south. To determine the direction towards the anomaly region, we fitted the excess muon region to a Gaussian function by dividing the region ($0 \leq \tan\theta_y < 1$) into four regions with a segment of 0.25 in $\tan\theta_y$, because the new structure seems to align along the $\tan\theta_y$ axis direction (Extended Data Fig. 2). The fitted centre value was used for triangulation and the errors of the estimated positions were defined from the errors on the sight lines coming from half of the bin width, that is, 0.0125 in $\tan\theta_x$ and 0.125 in $\tan\theta_y$ (Fig. 2g–i).

Scintillator hodoscopes from KEK. *Detector design.* The detector consists of two units of double layers, the *x* and *y* layers, of plastic scintillator arrays (Extended Data Fig. 3a–c). A single scintillator element is 10 mm × 10 mm in cross-section and 1,200 mm long. Each layer has 120 elements tightly packed, and hence its active area is 1,200 mm × 1,200 mm (Extended Data Fig. 3d). The element has a central hole along its length, through which a wave-shifter optical fibre is inserted to transfer the scintillation light efficiently to a multi-pixel photon counter sensor (Hamamatsu). The bias voltage of this counter sensor was selected according to the temperature of the Queen's chamber, which is constant regardless of the weather outside. Each layer has its own data acquisition box, which digitizes the information of sensor signals and sends them to a common personal computer inside the detector frame. The total power consumption of the detector system is 300 W. The vertical distance between the two units is 1,500 mm at position H1 and 1,000 mm at position H2, and gives an angular resolution around 7 mrad and 10 mrad, respectively. The tangent acceptance ranges from 0 (vertical) to 0.8 rad and 1.2 rad, respectively.

The detector introduces a dark cross-shaped artefact visible on the 2D histograms (Fig. 3a–d), which adds a small systematic error of 3% to the analysis. According to our analyses, the error is likely to be caused by the very narrow gap between neighbouring scintillator elements, but this effect has not been fully understood yet. This systematic error is not relevant in the present analysis, which examines only the existence of the new void.

Data acquisition. Raw data—time and position of all hit channels—are first stored in a personal computer and regularly retrieved with USB memory to be sent to KEK through the Internet. In the off-line analysis, a muon event is defined by the coincidence of the four layers, with at most two neighbouring hits in each of them. Events are accumulated in 2D bins (Δx, Δy) given by the channel number differences between the upper and lower layers along the *x* and *y* axes. The bin number hence ranges from −120 to 120 and provides the tangent of the incident angle when divided by 150 for position H1 and by 100 for position H2. We installed the detector at position H1 in August 2016, and continued the data acquisition for five months until January 2017. During this period, we accumulated 4.8 million events. We then moved the detector 2.9 m west to investigate the newly observed void better. The data acquisition will continue for more than eight months and 12.9 million events were accumulated at position H2 at the end of September 2017, with overall smooth acquisition for more than a year.

Data analysis and statistics. The first step of the analysis is the normalization of the data by a Monte Carlo simulation that takes into account the cosmic ray muon flux and muon interactions[35,36] (energy loss and multiple scattering) in the pyramid. We assume a constant energy loss[4] of 1.7 MeV per (g cm^{-2}), a mean density of 2.2 g cm^{-3}, and a radiation length of 26.5 g cm^{-2} for the stones. Muons are propagated in steps of 0.1 m. Because the known structures of the pyramid are simulated, their effects are removed after the normalization of the data and the remaining muon excess shows the existence of an unknown corridor-like new structure. The successful elimination of the known structures suggests the reliability of our simulation. Slices of the images along Δx are presented in Extended Data Fig. 4a and b. The vertical scale is the relative yield to the simulation result. The new structure can clearly be seen in each slice. The significance of the muon excess was obtained by a Gaussian fit: at position H1 the excess heights in the slices range from 5.2% to 8.9% and are higher than 10σ except for the outermost slice, in which the height is still greater than 5σ. At position H2 the height ranges from 8.9% to 11% and is again above 10σ except for the outermost slice, in which the excess is above 7σ. From these slices, we found that the structure starts almost at the centre of the pyramid and ends at an angle whose tangent is 0.8 to the north. As a result, the length of the main part of the new structure is approximately 30 m. Results from both positions H1 and H2 show that the new void is above the Grand Gallery, which is consistent with Nagoya's result.

Gas detectors from CEA. *Detector design.* A telescope (Extended Data Fig. 5a) is composed of 4 Micromegas (Extended Data Fig. 5b), a Micro-Pattern Gaseous Detector invented at CEA-Saclay[37] (Extended Data Fig. 5c). All the detectors

are identical, with an active area[12] of $50 \times 50\,cm^2$. They are built using bulk technology[38] with a screen-printing resistive film on top of the readout strips to allow for stable operation and higher gain[39]. Each detector provides x and y coordinates through a 2D readout inserted onto the printed circuit board (Extended Data Fig. 5d). The 1,037 readout strips (482 μm pitch) of each coordinate are multiplexed according to a patented scheme[40]. An argon–iC_4H_{10}–CF_4, non-flammable gas mixture (95–2–3) is flushed in series through all the detectors of a telescope, with a flow limited to below 0.5 litres per hour by a tight seal (measured gas leakage of less than 5 ml per hour per detector).

Each telescope is operated with a Hummingboard nano-computer running GNU/Linux, which controls all the electronics[12]: a dedicated high-voltage power supply card with five miniaturized modules (CAEN), which provide up to 2 kV with 12-V inputs, and the front-end unit readout electronics based on the DREAM ASIC[41]. A particularly important feature of DREAM is its self-triggering option to generate the trigger from the detectors themselves. A dedicated software package was developed to interface all these electronic components to the Hummingboard, which performs the data acquisition with the front-end unit. It also monitors and sets the high voltages through the high-voltage power supply and a patented amplitude feedback to keep the gain constant in spite of the extreme environmental conditions of the Giza plateau (Extended Data Fig. 5e–g). The overall consumption of a telescope is only 35 W.

A trigger is formed by the front-end unit when at least five coordinates out of eight observe a signal above a programmable threshold. The sampled signals (50 samples at a frequency of 100/6 MHz, Extended Data Fig. 5h) of all the electronic channels (64×8) are then directly converted to a ROOT file[42], a format commonly used in particle physics. The nano-computer performs the online reconstruction of muon trajectories, and the muon track parameters are sent to CEA in France with some environmental data (temperature, pressure, humidity in the gas) through a 3G connection.

Data acquisition. The data were collected from 4 May to 3 July 2017. Two telescopes were installed in front of the chevrons (north face), at a distance of 17 m and 23 m, respectively (Fig. 1b and c). The axis of both telescopes deviated slightly from the north–south axis, towards the east, to prevent the Grand Gallery from being at the centre of the image, where some correlated noise can show up. During acquisition time the two telescopes (called Alhazen and Brahic, at positions G1 and G2, see Fig. 1b and c) recorded 15.0 and 14.5 million triggers, respectively, from which 10.6 and 10.4 million track candidates were identified. After the χ^2 quality cut, 6.9 and 6.0 million good tracks were reconstructed, and form the images shown in Fig. 4a and d.

Data analysis and statistics. From the acquired tracks, we searched for anomalies by extracting slices in $\tan\phi$, that is, horizontal slices. To get more statistics, the thickness of the slices is larger than the binning shown in the 2D images. We chose a slice thickness of 0.10 for the Alhazen telescope, and we increased it to 0.11 for the Brahic telescope to keep roughly the same statistics. Extended Data Fig. 6 illustrates all the slices made with Alhazen from 0.21 to −0.19. From one histogram to another, the slice position is shifted by 0.02, which means the data of consecutive histograms largely overlap. The goal is to scan the pyramid and detect any deviation from statistics, whether fluctuations or not.

As can be seen in Extended Data Fig. 6, the slices show smooth distributions, except around histograms 5, 6 and 15. Histograms 6 and 15 correspond to Fig. 4b and c, respectively. These distributions were fitted with different functions, in particular polynomials. Though such functions are essentially empirical, a CRY/Geant4 simulation was performed to validate this choice further, leading to a good agreement using a second-order polynomial with a reduced χ^2 of 1.4. The same function reproduces data distributions fairly well—with a reduced χ^2 value of 1.6 and 2.0, respectively, for histograms 6 and 15—except in a region where an excess is clearly observed on both slices, with single-bin excesses of 4.2σ and 5.3σ respectively. Re-fitting with a second-order polynomial and a Gaussian significantly reduces the χ^2 to 1.2 and 1.4, with a Gaussian integral of 141.3 ± 28.3 (5.0σ, histogram 6) and 141.8 ± 24.7 (5.7σ, histogram 15). Similarly, Brahic data show two significant excesses, corresponding to Fig. 4e and f. A second-order polynomial alone results in a reduced χ^2 value of 1.8 and 2.4, respectively, while adding a Gaussian reduces them to 1.5 and 1.6. The Gaussian integral is 167.1 ± 44.6 (3.7σ, Fig. 4e) and 163 ± 26.5 (6.1σ, Fig. 4f).

The 3D model confirms that the (compatible) excesses from Fig. 4c (Alhazen) and 4f (Brahic) point to the same region of the pyramid and overlap very well with the Grand Gallery (Fig. 4h). The quasi-full overlap of the cones (owing to the purposeful proximity of the telescopes) justifies adding the two excesses, leading to 304.8 ± 36.2 (that is, 8.4σ). This fully validates the ability of the telescopes to unambiguously detect large structures in the core of the pyramid.

The 3D model also confirms that the excesses from Fig. 4b and e point to the same region. As before, the quasi-full overlap of the cones justifies adding the two excesses, leading to 308.4 ± 52.8 (5.8σ). A 3D comparison with the triangulation made by Nagoya University further confirms a large overlap of these regions. The other slices show no other anomaly exceeding 5σ.

It is worth mentioning that this analysis relies directly on raw data without model subtraction, which means the systematics are much smaller, and can only originate from the fitting function. As an exercise, a third-order polynomial fit was used for the histograms showing the new void, resulting in excesses of 5.2σ and 3.6σ for Alhazen and Brahic, and a combined excess of 303.5 ± 52.1 (5.8σ).

3D model of the pyramid. We designed an accurate 3D model of the pyramid by combining existing architectural drawings[34,43] photogrammetry[44], and laser scanner measurements[44], both inside and outside the pyramid. After merging these data, the model contains about 500,000 triangles (Extended Data Fig. 7b–d). This model was mainly used in the RTMS (see below) and as reference for the simplified models used in the other simulators. The full model has a precision of approximately 30 cm for the internal structures and approximately 1 m for the external casing.

Real-Time Muography Simulator. The RTMS (Extended Data Fig. 7a) is a fast, interactive simulator that was mainly used for preliminary analyses, to aid in positioning the gas sensors (telescopes), and for confirming the results obtained from the other simulators. It allows the user to place a sensor in the detailed 3D model of the pyramid and to simulate the observed muon rate in real time. Muon scattering is not simulated. For each pixel of the sensor, which represents a direction relative to the sensor, the simulator computes the opacity (integral of the density along the path) from the sensor to the outside of the pyramid, along this direction. We used a density of $2.2\,g\,cm^{-3}$ for the limestone, and $2.6\,g\,cm^{-3}$ for the granite. We consider that muons lose energy at a constant rate[4] of 1.69 MeV per ($g\,cm^{-2}$), which allows us to compute the minimal energy E_{min} to cross the pyramid given the value of the opacity. Finally, we use Miyake's formula[33] to calculate the distribution of muons that have greater energy than E_{min} coming in at a zenith angle θ. This value is computed for each pixel of the image, leading to a 2D histogram similar to those obtained with the detectors.

Data availability. The data that support the findings in this study are available from the corresponding authors on reasonable request.

29. Morishima, K. Latest developments in nuclear emulsion technology. *Phys. Proc.* **80,** 19–24 (2015).
30. Nishio, A. *et al.* Long term property of nuclear emulsion. *Progr. Proc. 1st Int. Conf. on 'Advanced Imaging' (ICAI2015)* 668–671 (Imaging Society of Japan, 2015).
31. Aoki, S. *et al.* The fully automated emulsion analysis system. *Nucl. Instrum. Methods B* **51,** 466–472 (1990).
32. Morishima, K. & Nakano, T. Development of a new automatic nuclear emulsion scanning system, S-UTS, with continuous 3D tomographic image read-out. *J. Instrum.* **5,** P04011 (2010).
33. Miyake, S. Rapporteur paper on muons and neutrinos. *13th Int. 'Cosmic Ray' Conf.* Vol. 5, 3638–3655 (1973).
34. Dormion, G. *La Chambre de Cheops: Analyse Architecturale* (Fayard, 2004).
35. Reyna, D. A simple parameterization of the cosmic-ray muon momentum spectra at the surface as a function of zenith angle. Preprint at https://arxiv.org/abs/hep-ph/0604145 (2006).
36. Jokisch, H., Carstensen, K., Dau, W., Meyer, H. & Allkofer, O. Cosmic-ray muon spectrum up to 1 TeV at 75 zenith angle. *Phys. Rev. D* **19,** 1368 (1979).
37. Giomataris, I. Y., Rebourgeard, P., Robert, J. P. & Charpak, G. MICROMEGAS: a high-granularity position-sensitive gaseous detector for high particle-flux environments. *Nucl. Instrum. Methods A* **376,** 29–35 (1996).
38. Giomataris, I. Y. *et al.* Micromegas in a bulk. *Nucl. Instrum. Methods A* **560,** 405–408 (2006).
39. Alexopoulos, T. *et al.* A spark-resistant bulk-micromegas chamber for high-rate applications. *Nucl. Instrum. Methods A* **640,** 110–118 (2011).
40. Procureur, S., Dupré, R. & Aune, S. Genetic multiplexing and first results with a $50 \times 50\,cm^2$ Micromegas. *Nucl. Instrum. Methods A* **729,** 888–894 (2013).
41. Flouzat, C. *et al.* Dream: a 64-channel front-end chip with analogue trigger latency buffer for the Micromégas tracker of the CLAS12 experiment. *Proc. TWEPP Conf.* https://indico.cern.ch/event/299180/contributions/1659618/contribution.pdf (2014).
42. Brun, R. & Rademakers, F. ROOT—an object oriented data analysis framework. *Nucl. Instrum. Methods A* **389,** 81–86 (1997).
43. Maragioglio, V. & Rinaldi, C. *L'Architettura delle Piramidi Menfite. Parte IV, La Grande Piramide di Cheope* (Rapallo, 1965).
44. Kraus, K. *Photogrammetry: Geometry from Images and Laser Scans* (Walter de Gruyter, 2007).

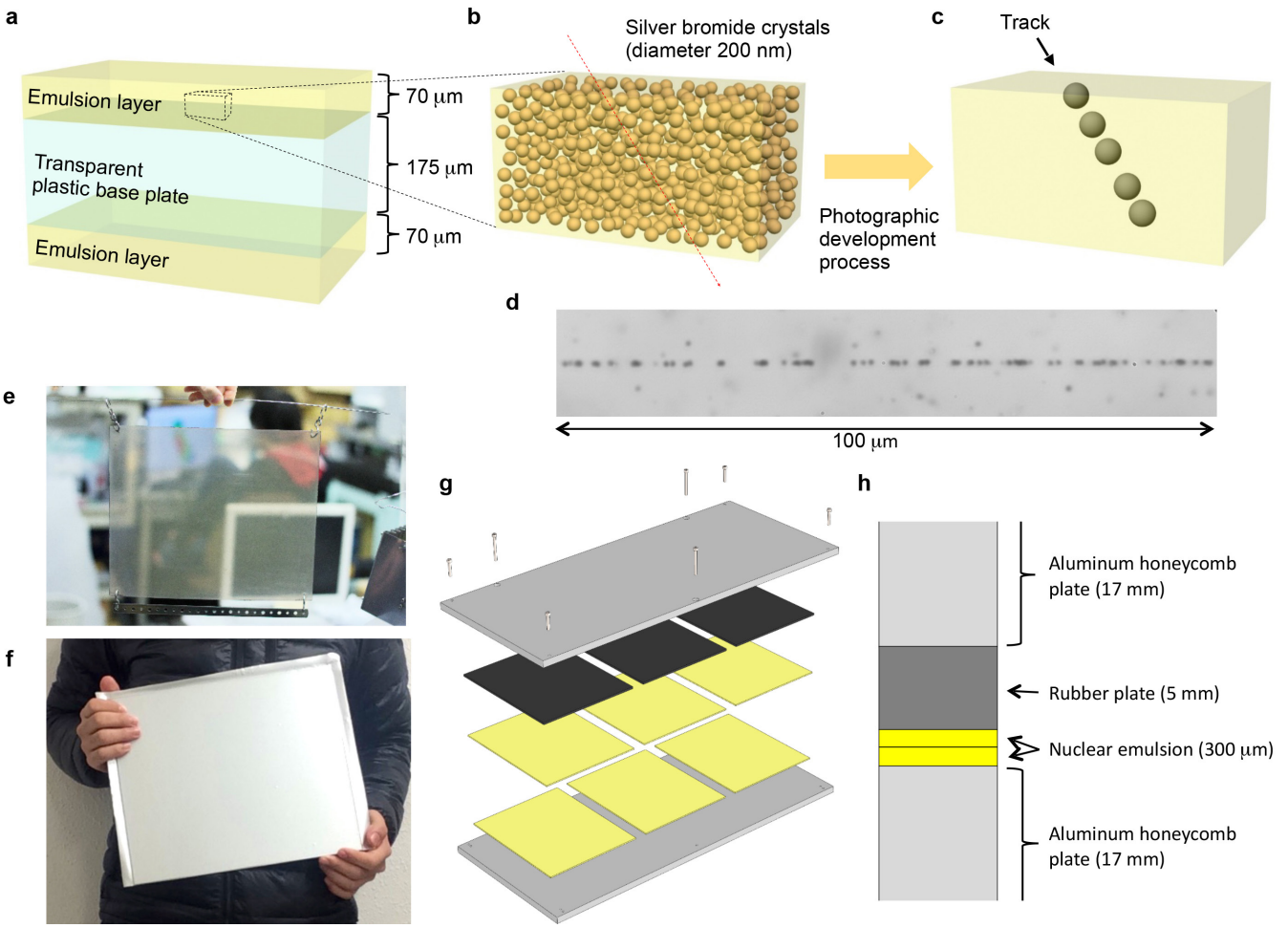

Extended Data Figure 1 | Overview of the nuclear emulsion films (Nagoya University). a, A cross-sectional schematic view of a nuclear emulsion. **b**, Enlarged schematic view of the emulsion layer. Silver bromide crystals are dispersed in gelatin. The red dashed arrow shows the trajectory of the charged particle. **c**, After the photographic development process, silver grains are aligned along the trajectory (track) of the charged particle. **d**, An optical microscopic photograph of the track of a minimum ionizing particle recorded in a nuclear emulsion. **e**, A nuclear emulsion after development. **f**, A vacuum-packed nuclear emulsion. **g**, Schematic view of the detector configuration: six packed nuclear emulsion films with a detection area of 30 cm × 25 cm each (yellow) are fixed between aluminium supporting plates (honeycomb plate, in grey). Two films stacked on top of each other are pressed with a rubber sheet (black) by four short screws. Three additional long screws are used as legs to correct the inclination of the detector. **h**, Cross-sectional schematic view of the nuclear emulsion detector as shown in **g**. Two packed films are stacked between two honeycomb plates and rubber sheet.

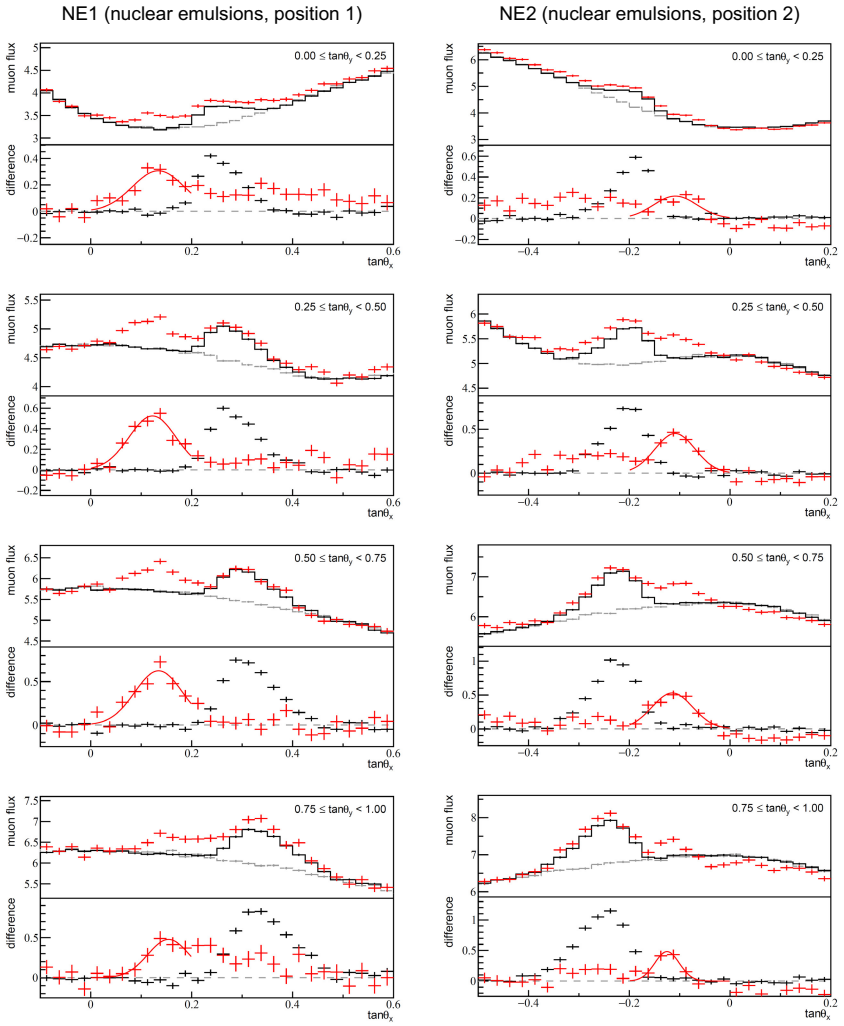

Extended Data Figure 2 | Slices of the data for the nuclear emulsion plates. Each panel shows slices for $\tan\theta_y$ every 0.25 units (in tangent) and separated into four ranges at $0 \leq \tan\theta_y < 1$ (see Fig. 2a–d). The top part of each panel shows muon flux distribution and the bottom part of each panel shows the difference of muon flux. In the top part of each panel, the red line shows the data, the black solid line shows the simulation with the internal structures, and the grey dashed line shows the simulation without any internal structure. In the bottom part of each panel, the red line shows the subtraction between the data and the simulation with the internal structures, and the black line shows subtraction between the simulation with and without the internal structures, so that the Grand Gallery appears as a muon excess. Error bars indicate statistical error of 1σ (standard deviation). The comparison between the excess that corresponds to the Grand Gallery and the one that corresponds to the new void shows that the two structures are of a similar scale. For each projection of difference of muon flux, we performed a Gaussian fitting to estimate the direction of anomalies. The fitting zone was $0 \leq \tan\theta_x \leq 0.2$ for position NE1 and $-0.2 \leq \tan\theta_x \leq 0$ for position NE2. These fitted centres were used for the triangulation.

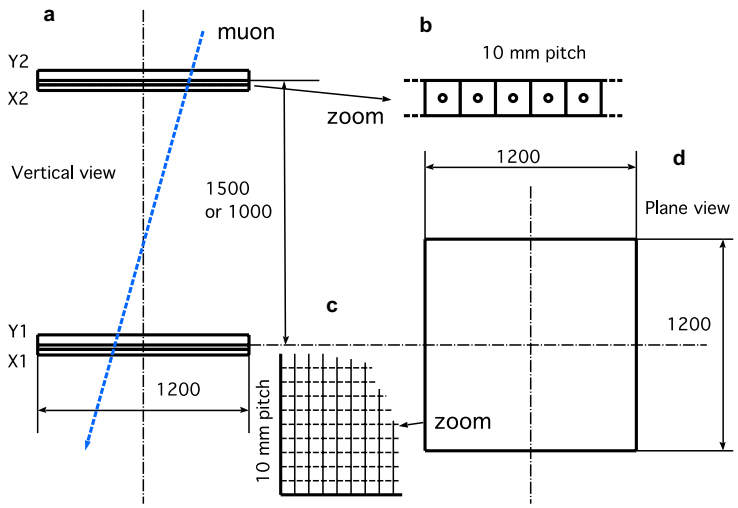

Extended Data Figure 3 | Overview of the scintillator hodoscopes (KEK). a, Vertical view of the detector, consisting of two units of orthogonal double scintillator layers. A blue arrow indicates a muon track passing through the whole instrument. **b**, Cross-section of a scintillator element, showing the central hole for the optical fibre. **c**, Grid made of double layers, detecting the position of incident muons. **d**, Plane view of the detector, with an active area of 1.2 m × 1.2 m.

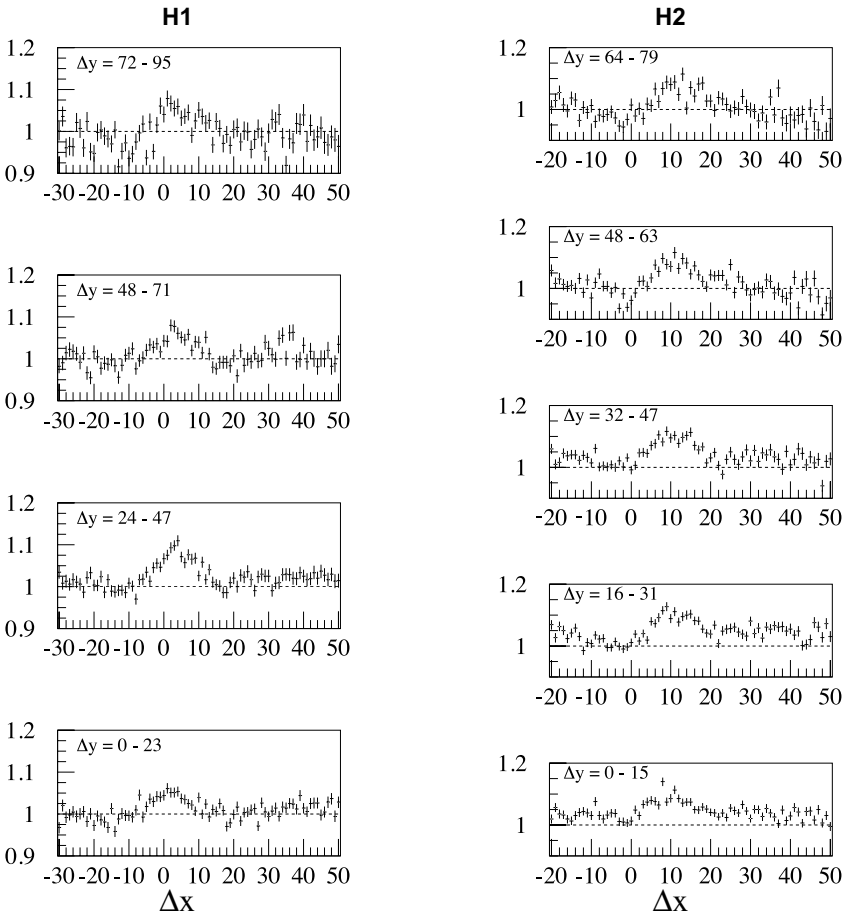

Extended Data Figure 4 | Slices of the data for the scintillator hodoscopes. Left, relative yield of the measurement to the simulation (including known structures) at position H1 for four slices (the width of each bin is 24 Δy). Right, relative yield at position H2 for five slices (the width of each bin is 16 Δy). Error bars show statistical errors of 1σ (standard deviation).

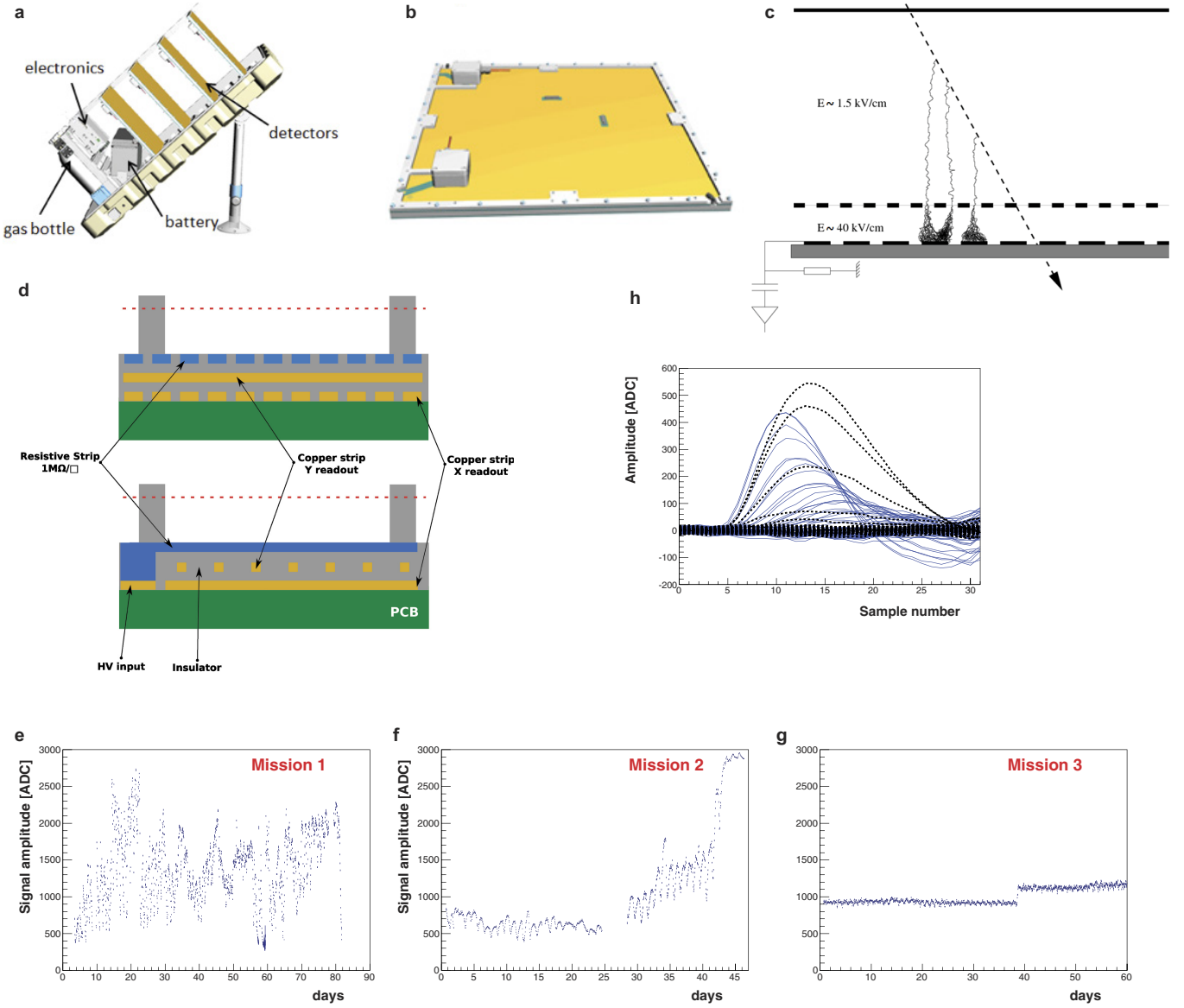

Extended Data Figure 5 | Overview of the gas detectors (CEA). **a**, Design of a telescope (without its cover) showing the four detectors, the electronics box, the battery and the gas bottles. **b**, Design of the multiplexed Micromegas detector. **c**, Principle of a Micromegas detector, showing the ionization and amplification of the signal initiated from a charged particle (dotted array). **d**, Layout of the detector with the micromesh in red, the resistive strip film in blue, and the Y and X copper readout strips in yellow. HV, high voltage; ADC, analogue digital converter. **e**–**g**, Amplitude variation of a detector in the Alhazen telescope as a function of time for two previous campaigns (ScanPyramids missions 1 and 2) and the one reported here (**g**), showing the effect of the patented feedback. Large variations (as observed in **e** and **f**) can lead to inefficiency or degraded resolution, and are totally absent from the data of this paper. The only step observed in **g** corresponds to a manual change of the target amplitude. **h**, Typical signal recorded in a detector, where each line corresponds to an electronic channel.

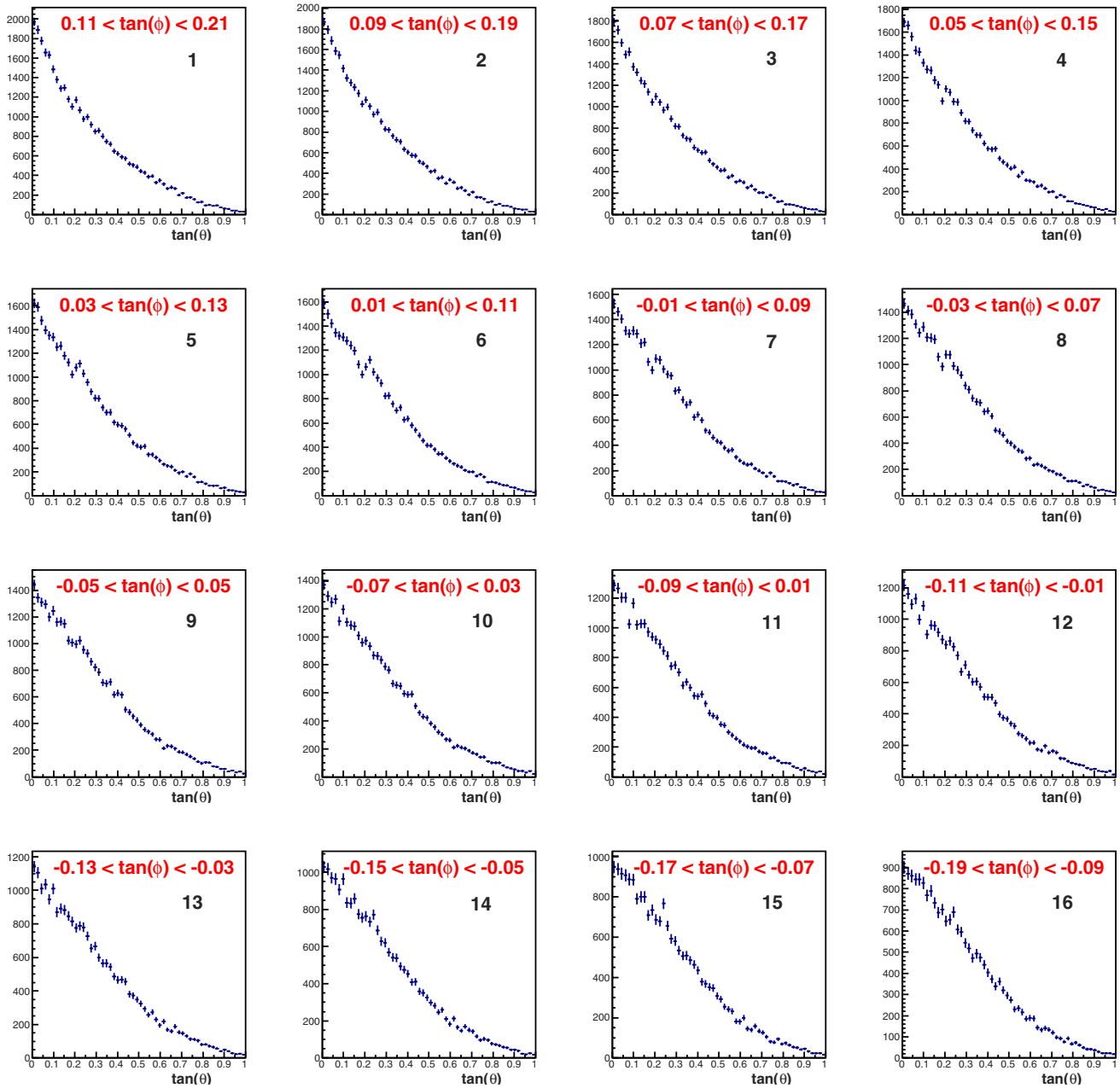

Extended Data Figure 6 | tanϕ, horizontal slices on the Alhazen muography. The slices are 0.10 (in tangent) thick, and each slice is shifted by 0.02 with respect to the previous one, which means they overlap. Distributions are generally smooth, with two large muon excesses on histograms 5, 6 and 15 (see Methods). Error bars show statistical error of 1σ (standard deviation).

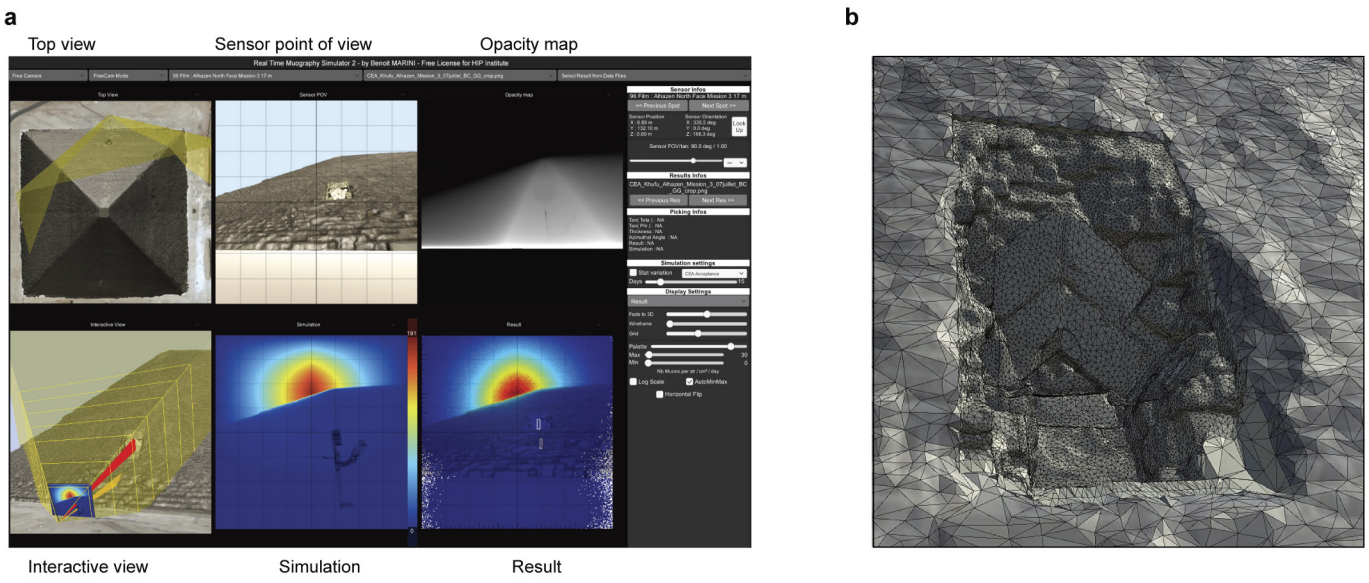

Extended Data Figure 7 | RTMS and 3D models. a, RTMS output, showing the CEA position G2 (Alhazen) sensor with a 6-view layout. Interactive view with display of sensor field of view and cone projections. Real-time simulation with internal structure overlaid in wireframe. Result with sensor point-of-view superposition. **b**, Zoom on chevron area (shaded wireframe). **c**, Enlarged view of optimized 3D model (shaded wireframe). **d**, Detail of optimized 3D model.

Extended Data Table 1 | Comparison of the three muon detection technologies

	Nuclear emulsion *Nagoya University*	**Hodoscopes** *KEK*	**Gas detectors** *CEA*
Angular Resolution	2-14mrad	7-10 mrad	0.8 - 4 mrad
Angular Acceptance	45 degrees	34 - 45 degrees	45 degrees
Active area (for this analysis)	30 cm x 25 cm / unit: 0.75 m x 0.6 m (NE1) 0.9 m x 0.5 m (NE2)	1.2 m x 1.2 m	50 cm x 50 cm
Position Resolution	1 μm	10 mm	400 μm
Height	0.2 mm	1-1.5 m	60 cm
Power requirement	No	Yes (300W)	Yes (35W)
Data taking	Need development	Real time	Real time